

# Inhomogeneous field quantum dot solar cell

Wenxi Lai\*

School of Applied Science, Beijing Information Science and Technology University, Beijing 100192, China

Structures of solar cells usually involve p-type and n-type bilayer materials until now. The p-n type structure can provide an asymmetric potential which causes charge carriers move in one definite direction and create bias voltage. In this paper, we prove theoretically that inhomogeneous light can be used to replace the p-n type structured materials in solar cells. In this protocol, asymmetric potential is provided by input light and working materials in the cell are allowed to be symmetrically structured. The inhomogeneous light creates polarization of electron number distribution in the conductance band of the cell and furthermore give rises to net current. Two conductor electrodes sandwiched with double quantum dots (QDs) have been used to demonstrate our model in the frame of non-equilibrium quantum master equation at room temperature. The double-QD opened system would be regarded as a basic component of the solar cell, then high current density and efficiency of such kind solar cell could be predicted. One advantage of the inhomogeneous field solar cell is that photocurrent can be obtained with lower cost and more simply structured devices.

PACS numbers: 73.63.Kv, 84.60.Jt, 72.40.+w, 73.23.Hk

Photovoltaic effect is one of the important ways to obtain green energy, which lead to fast development of research on solar cells. Solar cell technologies are classified into three generations [1, 2]. First generation solar cells are based on crystalline wafer of silicon [3, 4], including single/monocrystalline silicon solar cell [5], polycrystalline silicon solar cell [6] and amorphous silicon cells [2]. The first generation solar cells have advantage of higher conversion efficiency compared to the other types of cells, but have disadvantage of high costs at the same time [7]. Second generation solar cells are made from layers only a few micrometers thick films which is much thicker than crystalline silicon based cells [8]. Therefore, they are also called thin film solar cells. Since thin films can be packaged into flexible components and easily integrated onto a large, inexpensive substrate, the thin-film solar cells could provide more lower cost electricity in the market. The advantages of thin film cells are flexible and economical, however, they have drawback like the feature of low efficiency or toxicity [2]. The second generation solar cells are classified into three types, such as amorphous silicon thin film solar cell [1], cadmium telluride thin film solar cell [9] and copper indium gallium diselenide solar cells [10]. To change the situation of high costs in first generation solar cells and low efficiency in second generation solar cells, a series of new material based solar cells are emerged, call third generation solar cells.

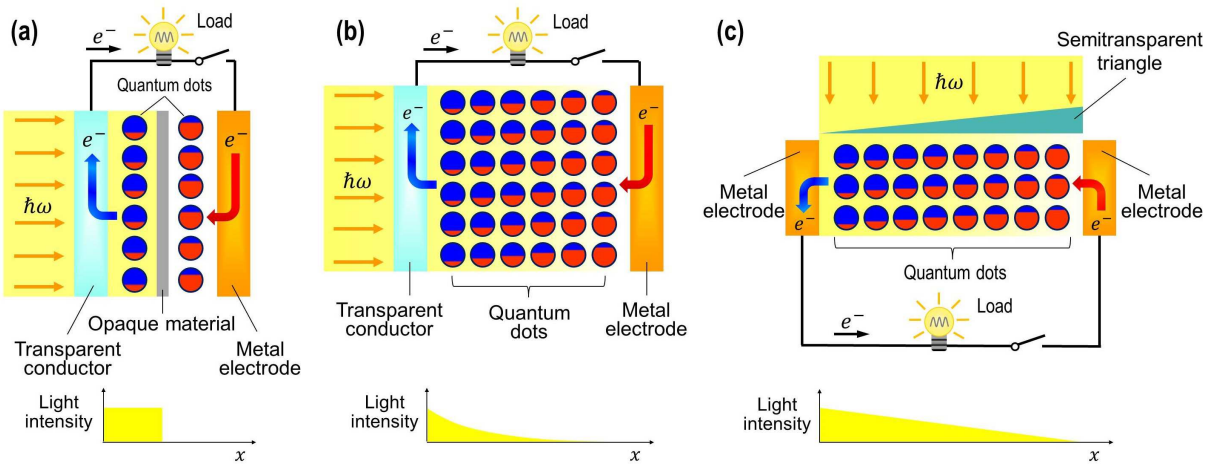


FIG. 1: (Color on line) Schematic illustration of inhomogeneous field QD solar cells. (a) Light intensity difference achieved through a non-transparent material sandwiched between two QDs layers. (b) QDs chip itself should create inhomogeneous optical field. (c) A semitransparent material is applied to obtain a light strength difference along the horizontal direction. The inhomogeneous field is illustrated with light intensity decrease along  $x$  axis.

\*Electronic address: wxlai@pku.edu.cn

Third generation solar cells do not rely on traditional p-n junctions, they are made from new developed sensitizing materials, such as dye molecules [11], QDs [12–14] and organic polymers [15]. These nano materials could help us to harvest light energy at low cost and low heat emission compared with the other two generation solar cells.

Actually, the third generation solar cells inherit some significant features of the first and second generation cells. For example, p-n type bilayer structure, integrability, thin film designs still play important role in recent research and development of nano material based solar cells [12–22]. Why p-type and n-type materials are important? Because the p-n junctions could provide potential difference to the cell system for the separation and collection of charge careers, such as electrons (negative), holes (positive) [23]. Task of light is just excite electrons into higher levels of nano crystals or molecules, then electrons and holes would be separated naturally due to the asymmetric potential of p-type and n-type bilayer.

In this paper, we proposed a new model of solar cell in which inhomogeneous light field is used to generate photocurrent in symmetrically designed conductor-QDs-conductor system without the p-n type materials. In this model, p-n type bilayer with asymmetric potential in a traditional solar cell is replaced by the inhomogeneous light with asymmetric field intensity. For a definite air mass (AM), power of light transferred to the earth surface is uniform. How to obtain spatially nonuniform light field is the key of the inhomogeneous light solar cell. In Fig. 1, three schemes for manufacturing such kind of cell systems are introduced. In Fig. 1 (a), two layers of QDs are separated by a opaque (non-transparent) film. As a result, light transmitted from the left side just acting on the left array of QDs and the right array of QDs are in the shadow of the opaque film. Although light can not transmit the opaque film, electrons are allowed to transmit it. Left electrode of the cell is a transparent conductor, right electrode is a ordinary metal conductor. A more simple structure is presented in Fig. 1 (b). Incident light from the transparent electrode is acting on QDs directly. Light would be reflected partially, absorbed partially and transmitted partially by the QDs and electrons. Therefore, light strength along its direction of propagation becomes weaker and weaker. It lead to different light powers at the left side and right side of the QDs film as soon as it thick enough. A more conservative design is given in Fig. 1 (c), where inhomogeneous light is created with a triangular shaped semitransparent material before the light propagate into the working area.

An electron in an opened QD can escape from the dot potential with a probability due to quantum tunneling. When the QD is sandwiched between two buck conductance (or semiconductor) with high Fermi energy level, the trapped electron would be blocked in the QD. However, light can determine distribution of electrons in their ground and excited states in QDs. Especially, the population of excited electrons would be determined by frequency and light intensity. When light intensity is different at left and right sides, electron distribution can be different at the two sides as shown in Fig. 1. It courses the population difference of excited electrons in left and right sides QDs. If Fermi level of the buck material is tuned between the ground state and excited state levels of QDs, net current of excited electrons can be achieved due to the population difference of excited electrons at two sides.

Compared with other solar cells, the configuration of inhomogeneous field solar cell is simply structured and it should be convenient to be popularized in the market. Since the p-type and n-type materials are neglected here, it can be more economical and flexible to integrate on a substrate. Furthermore, there is not particular toxic material is necessary for the cell.

The whole cell should be separated into a great number of unit components. Each unit is composed of neighboring double QDs. The rest of part can be regarded as environment of the double-QD system. In the following, a pair of neighboring QDs are considered to quantitatively describe photocurrent process in the cell. Motion of electrons under external light is illustrated in Fig. 2 (a)-(d). The double-QD system is coupled to left (L) and right (R) electrodes with the same Fermi level  $\varepsilon_F$ . If both of the two electrodes are conductors,  $\varepsilon_F > \varepsilon_C, \varepsilon_V$  and if both of the two electrodes are semiconductors,  $\varepsilon_C > \varepsilon_F > \varepsilon_V$ , where  $\varepsilon_C$  is the bottom level of conductance band and  $\varepsilon_V$  is top level of the valence band. The ground and excited levels of the QDs are denoted by  $\varepsilon_1$  and  $\varepsilon_2$ , respectively. They must satisfy  $\varepsilon_1 < \varepsilon_F < \varepsilon_2$  in this system as shown in Fig. 2. For Sun light inputs from the transparent electrode and directly interacts with the electron in left dot. Light intensity in the left dot is stronger than that in the right dot. For convenience, single-electron occupation in each QD is considered which works in strong Coulomb blockade regime. Furthermore, only the motion of electron would be described here, since every electron is mapping with a hole. The total Hamiltonian  $H$  can be separated into two parts for QDs  $H_{dot}$  and electrodes  $H_{pole}$ , namely,  $H = H_{dot} + H_{pole}$ . Neighboring two QDs that coupled to external light could be described in the single-particle Hamiltonian,

$$H_{dot} = \sum_{\alpha, s} \varepsilon_s n_{\alpha s} + \hbar \Lambda \sum_s (c_{Ls}^\dagger c_{Rs} + H.c.) + \hbar \sum_{\alpha} \frac{\Omega_{\alpha}}{2} (c_{\alpha 1}^\dagger c_{\alpha 2} e^{i(\omega t + \phi_{\alpha})} + H.c.). \quad (1)$$

Here,  $n_{\alpha s} = c_{\alpha s}^\dagger c_{\alpha s}$  represents occupation number operator of electron in state  $s$  in QD  $\alpha$  ( $\alpha = L, R$ ), where,  $s = 1$  and  $s = 2$  denote the ground and excited states of an individual electron, respectively. Electrons are allowed to tunnel from a left dot to the right dot with the rate  $\Lambda$ , and vice versa. Each QD is coupled to the input light with the Rabi frequency  $\Omega_{\alpha}$ . Any one frequency  $\omega$  of sun light is considered in the Hamiltonian and initial phase of the light is included in  $\phi_{\alpha}$  [24, 25].

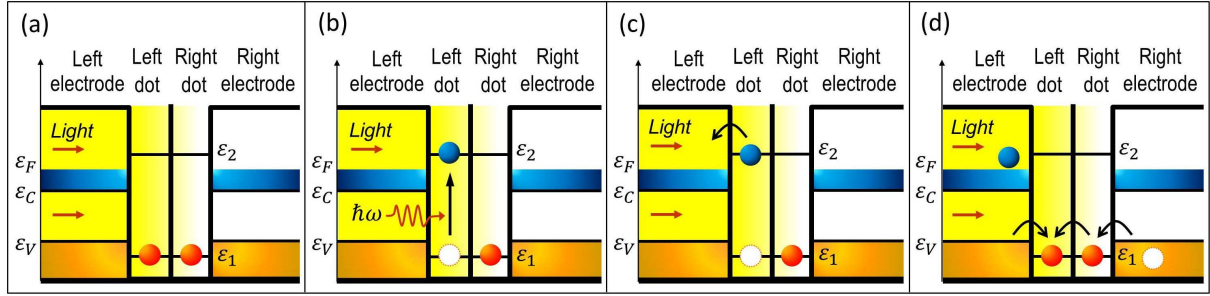


FIG. 2: (Color on line) Schematic display of inhomogeneous field double-QD solar cell. (a) Initially, electrons from the valence band enter the double-QD. (b) An electron in the left QD is driven by input light and excited to its higher energy state. (c) Due to Coulomb blockade effect, the excited electron have small probability to tunnel into the right QD, as a result, it would most likely transfer into conduction band of the left electrode. (d) Electrons from the valence band tunnel into the double-QD and then the system have returned to its original state of (a).

As conductance the electrodes could be described by the energy of free electron gas,

$$H_{pole} = \sum_{\alpha, k} \varepsilon_{\alpha k} n_{\alpha k} + \hbar g \sum_{\alpha, k, s} [a_{\alpha k}^\dagger c_{\alpha s} + H.c.]. \quad (2)$$

The first part of (2) describes energy of free electrons the left ( $\alpha = L$ ) and right ( $\alpha = R$ ) electrodes. Operator  $n_{\alpha k} = a_{\alpha k}^\dagger a_{\alpha k}$  represents occupation number of electrons with energy  $\varepsilon_{\alpha k}$  in the conductance or valance band. The third part represents coupling between electrodes and QDs. The tunneling amplitude  $g$  is considered to be insensitive to the electronic states  $s$  and the same for the left and right electrodes.

Using the total Hamiltonian  $H$  of the opened QDs system, equation of motion of electron due to the inhomogeneous sun light excitation can be derived under in the weak coupling limit of nano-device [24–26],

$$\frac{\partial \rho}{\partial t} = -\frac{i}{\hbar} [V_{dot}, \rho] + \mathcal{L}_L \rho + \mathcal{L}_R \rho, \quad (3)$$

which is a Lindblad form quantum master equation with the effective Hamiltonian

$$V_{dot} = \Delta \sum_{\alpha} n_{\alpha 2} + \hbar \Lambda \sum_s (c_{Ls}^\dagger c_{Rs} + H.c.) + \hbar \sum_{\alpha} \frac{\Omega_{\alpha}}{2} (c_{\alpha 1}^\dagger c_{\alpha 2} e^{i\phi} + H.c.) \quad (4)$$

for the QDs. The second and third term indicate the exchange of electrons between QDs and electrodes. The Lindblad super operators acting on the density matrix  $\rho$  can be written as

$$\mathcal{L}_L \rho = \frac{\Gamma}{2} \sum_s [f(\varepsilon_s) (c_{Ls}^\dagger \rho c_{Ls} - c_{Ls} c_{Ls}^\dagger \rho) + (1 - f(\varepsilon_s)) (c_{Ls} \rho c_{Ls}^\dagger - c_{Ls}^\dagger c_{Ls} \rho) + H.c.], \quad (5)$$

and

$$\mathcal{L}_R \rho = \frac{\Gamma}{2} \sum_s [f(\varepsilon_s) (c_{Rs}^\dagger \rho c_{Rs} - c_{Rs} c_{Rs}^\dagger \rho) + (1 - f(\varepsilon_s)) (c_{Rs} \rho c_{Rs}^\dagger - c_{Rs}^\dagger c_{Rs} \rho) + H.c.], \quad (6)$$

respectively. Single electron tunneling rate between a dot and an electrode is given by the energy independent coefficient  $\Gamma = 2\pi|g|^2 D(\varepsilon_s)$  under adiabatic approximation ( $D(\varepsilon_s)$  is density of states of electrons in any electrode at energy level  $\varepsilon_s$ ). Mean occupation number of the single-electron state with level  $\varepsilon_s$  in any electrode is given by the Fermi-Dirac distribution function  $f(\varepsilon_s) = \frac{1}{e^{(\varepsilon_s - \varepsilon_F)/k_B T} + 1}$  at equilibrium temperature  $T$  and Fermi level  $\varepsilon_F$ .

Considering single-electron transit in a QD, three states would be involved in each dot, empty state  $|0\rangle_{\alpha}$ , occupation of a ground state electron  $|1\rangle_{\alpha}$ , and occupation of an excited state electron  $|2\rangle_{\alpha}$ . Mean occupation number of the single-electron state  $|s\rangle_{\alpha}$  in QD  $\alpha$  (left or right) can be defined as  $P_{\alpha 0} = \text{tr}\{c_{\alpha s} c_{\alpha s}^\dagger \rho\}$ ,  $P_{\alpha 1} = \text{tr}\{c_{\alpha 1}^\dagger c_{\alpha 1} \rho\}$ ,  $P_{\alpha 2} = \text{tr}\{c_{\alpha 2}^\dagger c_{\alpha 2} \rho\}$ , respectively. They are determined by the equation of motion (3). tr here represents trace over the 9 double-QD states  $\{|s\rangle_L |r\rangle_R \mid s, r=0, 1_1, 1_2\}$ .

Defining the total occupation number of electrons in the double-QD at time  $t$  by  $N(t) = \sum_{\alpha, s} \text{tr}\{n_{\alpha s} \rho(t)\}$ , current in the unit component could be calculated using the continuity equation[27–29]:

$$-e \frac{dN(t)}{dt} = j_L - j_R, \quad (7)$$

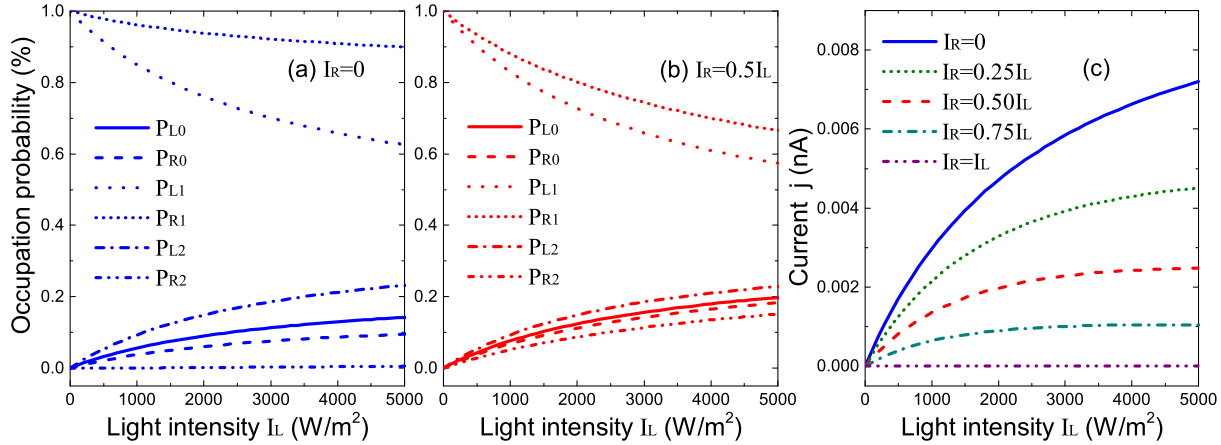


FIG. 3: (Color on line) (a) Mean occupation of numbers of electrons at different states in the left and right QD with  $I_R = 0$ . (b) Mean occupation numbers of electrons in the left and right QD with  $I_R = 0.5I_L$ . (c) Current of the double-QD unit component under given inhomogeneous fields.

where  $j_L$  and  $j_R$  denotes left and right sides currents of the double-QD system. According to Kirchhoff's Laws, left and right currents should satisfy  $j_L - j_R = 0$  in stationary circuit. Therefore, current through system can be written as  $j = (j_L + j_R)/2$ . Here, direction of the positive current is defined to be from left to right. Substituting Eq. (3) into the continuity equation(7), expressions of the current  $j$  can be reached in the form [26]

$$j = -e \frac{\Gamma}{2} \sum_s [f(\varepsilon_s)(P_{L0} - P_{R0}) - (1 - f(\varepsilon_s))(P_{Ls} - P_{Rs})]. \quad (8)$$

What we know from Eq. (8) is that net current  $j$  in the cell is directly caused by the polarization (the difference of mean occupation number) of the electron number distribution in the neighboring QDs. To understand the current formula (8), we could write it in the conceptual relation as [30],

$$j = \frac{Q}{\tau}, \quad (9)$$

where  $Q = -e \sum_s [f(\varepsilon_s)(P_{L0} - P_{R0}) - (1 - f(\varepsilon_s))(P_{Ls} - P_{Rs})]$  is the polarization of inversion charge in the double-QD system,  $\tau = \frac{2}{\Gamma}$  is the electron transit time from one electrode to the other electrode through QDs.

Current (8) may be numerically calculated associated with the solutions of Eq. (3) under the normalization constraint  $tr\rho = 1$ . The basic parameters in Eq. (3) are taken in the range of practical dates as  $\Gamma = 0.01 \sim 10$  GHz [31–33],  $\Lambda = \Gamma$ ,  $T = 300$  K,  $\varepsilon_e - \varepsilon_g = 0.4 \sim 4$  eV (for QD radius  $3 \sim 50$  nm) [34],  $\lambda = 400 \sim 760$  nm [2], respectively. In addition, the Rabi frequency  $\Omega_\alpha = \frac{|\varphi_{12}|E_\alpha}{\hbar}$  is proportional to electric field amplitude  $E$  and the absolute value of dipole moment  $\varphi_{12}$ . For the semiconductor QD, dipole moment is around  $\varphi_{12} = 30 \sim 90$  D [35–37] for different material and dimensions. In this way, the Rabi frequency can be connected to the light intensity as  $\Omega_\alpha = \frac{|\varphi_{12}|}{\hbar} \sqrt{\frac{2c\mu_0 I_\alpha}{n}}$  for  $\alpha = L$  and  $\alpha = R$ . According to electromagnetic field theory, light intensity  $I_\alpha$  in dot  $\alpha$  is proportional to square of electric field amplitude  $E_\alpha$ , namely  $I_\alpha = \frac{n}{2c\mu_0} |E_\alpha|^2$ , where  $n$  is refractive index,  $c$  is speed of light, and  $\mu_0$  is permeability of vacuum. The refractive index is taken with a typical value  $n = 3$  of semiconductor [38, 39]. After sunlight travels through the earth's atmosphere to the earth's surface, it's intensity is reduced to nearly  $1000$  W/m<sup>2</sup> which is called 1 sun. Basic parameters used in this work are  $\mu = 70$  D,  $\Gamma = \Lambda = 0.5$  GHz,  $\phi = 0$ ,  $n = 3.0$ ,  $T = 300$  K,  $\varepsilon_e - \varepsilon_g = 1.77$  eV unless some of them are taken as variables in a figure. In resonant absorbtion ( $\Delta = 0$ ),  $\hbar\omega = 1.77$  eV is corresponding to a photon with wavelength  $\lambda = 700$  nm.

According to the theory of light-matter interaction in quantum optics [24, 25], it is not hard to understand that when frequency of light matches to transition energy of electrons, light intensity determine probability of electrons on its excited state due to the relation  $\Omega_\alpha \propto \sqrt{I_\alpha}$ . In Fig. 3, Mean occupation numbers of single-electron states in left and right QD are shown as a function of input light intensity  $I_L$ . Without incident light,  $I_L = 0$ , both the two QDs are fully occupied by the ground state electrons, with  $P_{L1} = P_{R1} = 1$ . When light is entering with different intensities in the left and right QDs, the cell would begin to work. In Fig. 3 (a), light intensity  $I_L$  in the left QD is set to be the same as the incident light. However, light in the right QD is assumed to be zero  $I_R = 0$ . The fact is that light is only interacting with the left QD electron and there is negligible light in the right QD, the occupation probabilities

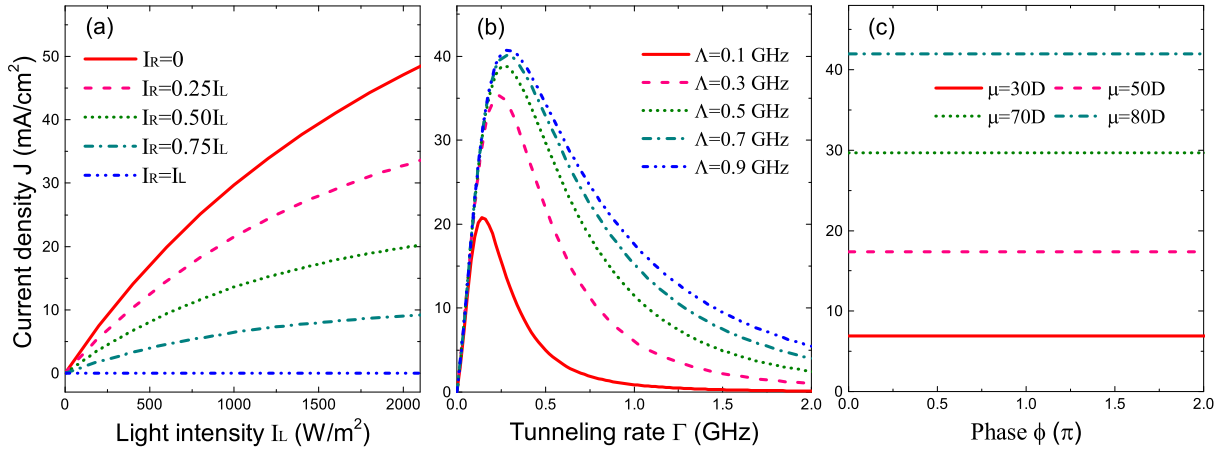


FIG. 4: (Color on line) (a) Current densities for the change of input light intensity in the left  $I_L$  and right  $I_R$  QDs. (b) Current densities versus electron tunneling rate  $\Gamma$  for different inter-dot tunneling rates, where  $I_L = 1000$  W/m<sup>2</sup> and  $I_R = 0$ . (c) Current densities as a function of light phase  $\phi$  at different dipole moments, where  $I_L = 1000$  W/m<sup>2</sup> and  $I_R = 0$  W/m<sup>2</sup>.

of excited electron in left QD is much larger than that in right QD, namely  $P_{L2} \gg P_{R2}$  with  $P_{R2} \rightarrow 0$ . At the same time, probability of empty occupation in left QD is larger than that in right QD,  $P_{L0} > P_{R0}$ . Corresponding current in the double-QD is given in Fig. 3 (c) with the solid the same colored blue line. When light intensity in the right QD is half of the intensity in the left QD,  $I_R = I_L/2$ , the mean occupation number of electron in the right dot excited level is remarkably increased, satisfying  $P_{L2} > P_{R2}$ . Corresponding current is plotted in Fig. 3 (c) with the same red colored line. What we know from Fig. 3 is that the increase of light strength in the right QD decreases current. It reveals the significance of light intensity difference induced electron occupation difference in the cell.

Now, we estimate current and efficiency of the whole inhomogeneous field solar cell based on the above double-QD unit component. The whole cell is composed of a QDs film sandwiched between two conductors as illustrated in Fig. 1. Then, current density  $J$  of the solar cell could be calculated as

$$J = \sigma j, \quad (10)$$

where  $j$  represents current through the single unit component and  $\sigma$  denotes surface density of the unit component. Here,  $\sigma$  would be taken as the sheet density of QDs. The sheet QD density commonly ranged from  $10^9$  cm<sup>-2</sup> to  $10^{11}$  cm<sup>-2</sup> which can be controlled by QD growth techniques [40–42]. Here, a typical value of  $\sigma = 8 \times 10^9$  cm<sup>-2</sup> has been taken in the numerical treatments.

Considering the whole cell, current densities in the inhomogeneous field photovoltaic system have been plotted in Fig. 4. Current increase can be observed for the larger incident light intensity as illustrated in Fig. 4 (a). Obviously, the bigger difference of light intensity in the left and right QDs, the larger current can be obtained for definite input light. As manifested in the figures, current densities in the inhomogeneous field cell can be comparable to the traditional p-n type material based solar cells [11–18, 21, 22, 43–46]. The rates of electron tunneling  $\Gamma$  and  $\Lambda$  determine the characteristic time of electron transit. However, they also play different roles in the system as shown in Fig. 4 (b). When  $\Gamma$  is very small, electrons are hard to exchange between electrodes and QDs, which would depress current. When  $\Gamma$  is too large, polarization of electron number distribution in the neighboring QDs hard to be constructed, which affects the creation of voltage and net current. As a result, currents have top values for the change of  $\Gamma$ . As the inter-QD coupling strength,  $\Lambda$ , increase of  $\Lambda$  always improves current. Although our results are achieved with the model using coherent light, the inhomogeneous field solar cell should work under sun light which has much short coherent time. It is demonstrated in Fig. 4 (c) that current in the system is insensitive to the phase  $\phi$  of light. Fig. 4 (c) also reflects importance of the dipole moment  $\mu$  of QDs for photocurrent creation. It is not surprising that since the Rabi frequency  $\Omega_\alpha$  is actually proportional to the dipole moment  $\mu$  of materials.

Next, let us try to calculate photocurrent efficiency of the cell. Current of electron through an area  $S$  of the cell could be calculated as  $I_e = JS$ . Corresponding power is equal to  $P_e = I_e U_e$ , where the voltage  $U_e$  should be related to the energy change of electron in the cell, namely energy level difference,  $\varepsilon_2 - \varepsilon_1$ , of the QD. Therefore, we have  $U_e = (\varepsilon_2 - \varepsilon_1)/e$ . Power of light  $P_L$  on the area  $S$  is equal to  $P_L = I_L S$ . From the electron current power and light power, we may calculate the efficiency of the inhomogeneous field solar cell through the formula,

$$\eta = \frac{P_e}{P_L} \times 100\%. \quad (11)$$

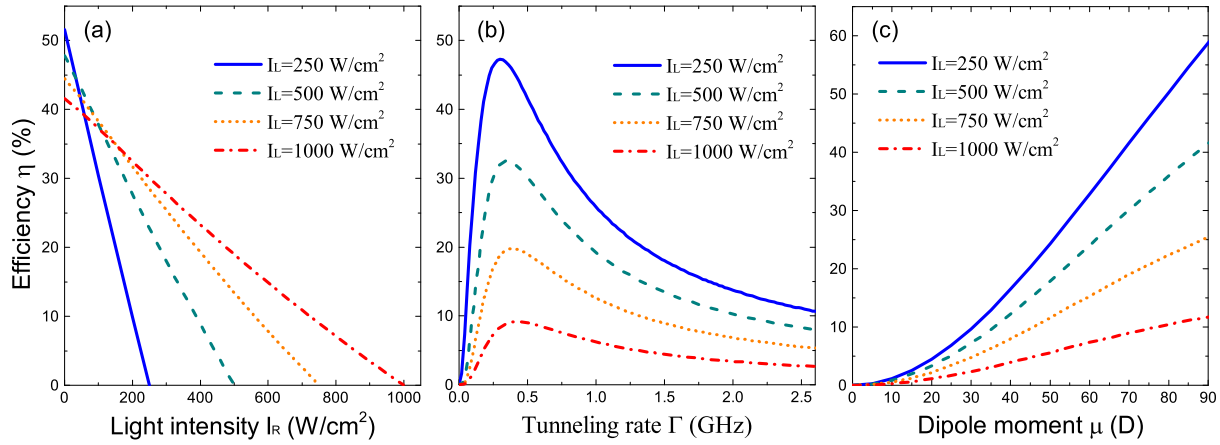


FIG. 5: (Color on line) (a) Light difference dependent cell efficiencies under four given strengths of incident light. (b) Cell efficiencies versus electron tunneling rate. (c) Dipole momentum dependent cell efficiencies. In (b) and (c), the input light intensity is set to be  $I_L = 1000 \text{ W/m}^2$ .

The values of efficiency based on Eq. (11) have been shown in Fig. 5 versus several parameters of this system. Fig. 5 (a) illustrates linear relationship between light intensity difference  $I_L - I_R$  in neighboring QDs and the photocurrent efficiency  $\eta$ . Similar to the behavior of current density, efficiency has a highest value for the electron transit rate  $\Gamma$  (see Fig. 5 (b)). The demand for top value of efficiency on the transit rate  $\Gamma$  is lower than  $1\text{GHz}$ . Many semiconductor QD materials can satisfy this condition [31–33]. In addition, due to the dipole moment determines the strength of interaction between electronic system and light, efficiency of energy conversion from light to electrons benefits from large dipole moment as plotted in Fig. 5 (c). Efficiency of the inhomogeneous field QD solar cell is not lower than QD based solar cells with the p-n bilayer type materials, such as QD-Dye bilayer-sensitized solar cell [11], InAs/GaAs quantum dot thin film solar cell [13, 14], molecules mediated colloidal QD solar cell [15], QD homojunction solar cells [18], hybrid GaAs solar cell [21], multilayer colloidal QD solar cell [44] and so on.

Finally, we discuss about the absorbtion of sun light. In our model, we just considered single transition energy of QDs, namely  $\varepsilon_2 - \varepsilon_1$ . At the same time, in the light-matter interaction, light intensity of 1 sun ( $1000 \text{ Wm}^{-2}$ ) is considered. In fact, sun light consists of electromagnetic field with large range of wavelengths. Therefore, if all QDs in the cell have just one transition as considered in the present model, light effectively absorbed by the cell would be much weaker than the value  $1000 \text{ Wm}^{-2}$ . As a result, current density and efficiency of the photovoltaic system should be very small as manifested in the above figure. Fortunately, there are some direct methods to supplement our present model for more higher current and efficiency. Firstly, practical QDs are usually characterized by quantized energy of multilevels, which reveals more than one transitions are allowed actually for the excitation of more electrons. Secondly, multiple exciton effect in QDs can increase photocurrent. In the multiple exciton process, a single photon with large energy can excite two or more electrons in a QD[46, 47]. Thirdly, density of QDs considered in our model can be raised by at least 10 or  $10^2$  times, which could increase the absorbtion ability of the QD films.

In conclusions, we have proposed a model of inhomogeneous light QD solar cell, which is different from the p-n type material based solar cells. In p-n type material based solar cells, there would be asymmetric potentials constructed by the p-type and n-type materials. However, in the present inhomogeneous light solar cell, materials can be characterized by symmetric potentials, the thin films arranged in the cell are allowed to be both the same semiconductors or the electrodes. As a cost, the asymmetry comes external light which is distributed with inhomogeneous intensity in the cell materials. Using the model of two neighboring QDs coupled to two electrodes respectively, the inhomogeneous light QD solar cell is proved theoretically. Under the input light coupling, excited electrons have more probabilities to be collected in the left QDs, which give rise to net current in the conduction band of electrodes. The polarization of electron number distribution in the double-QD system is at the heart of the mechanism of this cell. Considering large array of QDs on a film, current densities and cell efficiencies are calculated under several important parameters, such as dipole moment of QDs, electron transit rate, and light intensity difference in QDs. The features of the cell on these parameters are show that current density and efficiency of this kind of solar cell have large flexibility to be tuned in practice.

### Acknowledgments

This work was supported by the Scientific Research Project of Beijing Municipal Education Commission (BMEC) under Grant No.KM202011232017.

---

[1] Sharma, S. et al. Solar Cells: In Research and Applications-A Review. *Materials Sciences and Applications* **6**, 1145-1155 (2015).

[2] Ranabhat, K. et al. An introduction to solar cell technology. *Journal of Applied Engineering Science* **405**, 481-491 (2018).

[3] Choubey, P. C. et al. A Review: Solar Cell Current Scenario and Future Trends. *Recent Research in Science and Technology*, **4**, 99 (2012).

[4] Bagher, A. M. et al. Types of Solar Cells and Application. *American Journal of Optics and Photonics* **3**, 94-113 (2015).

[5] Srinivas, B. et al. Review on Present and Advance Materials for Solar. *International Journal of Engineering Research-Online*, **3**, 178-182 (2015).

[6] Saga, T. et al. Advances in Crystalline Silicon Solar Cell Technology for Industrial Mass Production. *NPG Asia Materials*, **2**, 96-102 (2010).

[7] Green, M. A. et al. Solar cell efficiency tables: version 48. *Prog. Photovoltaics*, **24**, 905-913 (2016).

[8] Chopra, K. L. et al. Thin-Film Solar Cells: An Overview. *Prog. Photovoltaics*, **12**, 69-92 (2004).

[9] Badawy, W. A. et al. A Review on Solar Cells from Si-Single Crystals to Porous Materials and Quantum Dots. *Journal of Advanced Research*, **6**, 123-132 (2015).

[10] Razýkov, T. M. et al. Solar Photovoltaic Electricity: Current Status and Future Prospects. *Solar Energy*, **85**, 1580-1608 (2011).

[11] Shalom, M. et al. Quantum Dot-Dye Bilayer-Sensitized Solar Cells: Breaking the Limits Imposed by the Low Absorbance of Dye Monolayers. *J. Phys. Chem. Lett.* **1** 1134-1138 (2010).

[12] Hu, L. et al. Flexible and efficient perovskite quantum dot solar cells via hybrid interfacial architecture. *Nature Commun.* **12** 466 (2021).

[13] Tutu, F. K. et al. InAs/GaAs quantum dot solar cell with an AlAs cap layer. *Appl. Phys. Lett.* **102** 163907 (2013).

[14] Sogabe, T. et al. Enhancement of current collection in epitaxial lift-off InAs/GaAs quantum dot thin film solar cell and concentrated photovoltaic study. *Appl. Phys. Lett.* **105** 113904 (2014).

[15] Baek, S.-W. et al. Efficient hybrid colloidal quantum dot/organic solar cells mediated by near-infrared sensitizing small molecules. *Nature Energy* **4** 969-976 (2019).

[16] Cheriton, R. S. et al. Two-photon photocurrent in InGaN/GaN nanowire intermediate band solar cells. *Commun. Materials* **1** 63 (2020).

[17] Shi, G. et al. The effect of water on colloidal quantum dot solar cells. *Nature Commun.* **12** 4381 (2021).

[18] Stavrinadis, A. et al. Heterovalent cation substitutional doping for quantum dot homojunction solar cells. *Nature Commun.* **4** 2981 (2013).

[19] Ramiro, I. et al. Analysis of the intermediate-band absorption properties of type-II GaSb/GaAs quantum-dot photovoltaics. *Phys. Rev. B* **96** 125422 (2017).

[20] Beard, M. C. et al. Multiple Exciton Generation in Semiconductor Quantum Dots. *J. Phys. Chem. Lett.* **2** 1282-1288 (2011).

[21] Han, H.-V. et al. A Highly Efficient Hybrid GaAs Solar Cell Based on Colloidal-Quantum-Dot-Sensitization. *Scientific Report* **4** 5734 (2014).

[22] Lin, C.-C. et al. Highly efficient CdS-quantum-dot-sensitized GaAs solar cells. *Optics Express* **20** A319-A326 (2012).

[23] Nozik, A. J. et al. Quantum dot solar cells. *Physica E* **14** 115-120 (2002).

[24] Meystre, P. and Sargent III, M. Elements of Quantum Optics. Fourth edition, Springer (2007)

[25] Scully, M. O. and Zubairy, M. S. Quantum Optics. Cambridge University Press, Cambridge (1997)

[26] Delerue, C. and Lannoo, M. Nanostructure: Theory and Modelling, Springer-Verlag, Berlin Heidelberg (2004)

[27] Davies, J. H. et al. Current and rate equation for resonant tunneling. *Phys. Rev. B* **47**, 4603 (1993).

[28] Jauho, A. P. et al. Time-dependent transport in interacting and noninteracting resonant-tunneling systems. *Phys. Rev. B* **50**, 5528 (1994).

[29] Twamley, J. et al. Spin-detection in a quantum electromechanical shuttle system. *New J. Phys.* **8**, 63 (2006).

[30] Puers, R. et al. Nanoelectronics: Materials, Devices, Applications, Wiley-VCH, Weinheim (2017)

[31] Sargent, E. H. et al. Colloidal quantum dot solar cells. *Nat. Photon.* **6**, 133-135 (2012).

[32] Sanehira, E. M. et al. Enhanced mobility CsPbI<sub>3</sub> quantum dot arrays for record-efficiency, high-voltage photovoltaic cells. *Sci. Adv.* **3**, 4204 (2017).

[33] Kamat, P. V. et al. Quantum Dot Solar Cells. Semiconductor Nanocrystals as Light Harvesters. *J. Phys. Chem. C* **112**, 18737-18753 (2008).

[34] Jasim, K. E. et al. Quantum Dots Solar Cells. InTechOpen (2018).

[35] Kamada, H. et al. Exciton Rabi Oscillation in a Single Quantum Dot. *Phys. Rev. Lett.* **87**, 246401 (2001).

[36] Stievater, T. H. et al. Rabi Oscillations of Excitons in Single Quantum Dots. *Phys. Rev. Lett.* **87**, 133603 (2001).

[37] Ares, N. et al. SiGe quantum dots for fast hole spin Rabi oscillations. *Appl. Phys. Lett.* **103**, 263113 (2013).

- [38] Ravindra, N. M. et al. Energy gap-refractive index relations in semiconductors-An overview. *J. Choi, Infrared Physics & Technology* **50**, 21-29 (2007).
- [39] Tripathy, S. K. et al. Refractive indices of semiconductors from energy gaps. *Optical Materials* **46**, 240-246 (2015).
- [40] Li, T. et al. Challenges to the concept of an intermediate band in InAs/GaAs quantum dot solar cells. *Appl. Phys. Lett.* **103**, 141113 (2013).
- [41] Wigger, D. et al. Rabi oscillations of a quantum dot exciton coupled to acoustic phonons: coherence and population readout. *Optica* **5**, 1442-1450 (2018).
- [42] Kasprzak, J. et al. Vectorial nonlinear coherent response of a strongly confined exciton-biexciton system. *New J. Phys.* **15**, 055006 (2013).
- [43] Cress, C. D. et al. Quantum dot solar cell tolerance to alpha-particle irradiation. *Appl. Phys. Lett.* **91**, 183108 (2007).
- [44] Lee, S. et al. Orthogonal colloidal quantum dot inks enable efficient multilayer optoelectronic devices. *Nature Commun.* **11** 4814 (2020).
- [45] Cao, Y. et al. The role of surface passivation for efficient and photostable PbS quantum dot solar cells. *Nature Energy* **1** 16035 (2016).
- [46] Nozik, A. J. et al. Semiconductor Quantum Dots and Quantum Dot Arrays and Applications of Multiple Exciton Generation to Third-Generation Photovoltaic Solar Cells. *Chem. Rev.* **110** 6873-6890 (2010).
- [47] Pusch, A. et al. Microscopic reversibility demands lower open circuit voltage in multiple exciton generation solar cells. *Appl. Phys. Lett.* **118** 151103 (2021).